Radial Compression of an Antiproton Cloud for Production of Intense Antiproton Beams

N. Kuroda,[1,2] H. A. Torii,[2] M. Shibata,[1] Y. Nagata,[2] D. Barna,[3] M. Hori,[4,5] D. Horváth,[3] A. Mohri,[1] J. Eades,[5] K. Komaki,[2] and Y. Yamazaki[1,2]

[1]*Atomic Physics Laboratory, RIKEN, Wako-shi, Saitama 351-0198, Japan*
[2]*Institute of Physics, University of Tokyo, Komaba, Meguro-ku, Tokyo 153-8902, Japan*
[3]*KFKI Research Institute for Particle and Nuclear Physics, H-1121 Budapest, Hungary*
[4]*Max-Planck-Institute für Quantenoptik, Hans-Kopfermann-Strasse 1, D-85748, Garching, Germany*
[5]*Department of Physics, University of Tokyo, Hongo, Bunkyo-ku, Tokyo 113-0033, Japan*

(Received 1 October 2007; published 19 May 2008)

We report here the radial compression of a large number of antiprotons ($\sim 5 \times 10^5$) in a strong magnetic field under ultrahigh vacuum conditions by applying a rotating electric field. Compression without any resonant structures was demonstrated for a range of frequencies from the sideband frequency of 200 kHz to more than 1000 kHz. The radial compression achieved is a key technique for synthesizing and manipulating antihydrogen atoms and antiprotonic atoms.

DOI: 10.1103/PhysRevLett.100.203402 PACS numbers: 36.10.−k, 37.20.+j, 52.27.Jt

Cooling and manipulation of a large number of antiprotons held in an electromagnetic trap are key techniques for synthesizing antihydrogen atoms and antiprotonic atoms [1–3]. In our previous Letter [3], we reported accumulation and cooling of antiprotons in an electromagnetic trap with at least 50 times higher efficiency than has been achieved by conventional methods. Extracting these antiprotons from the trap and transporting them efficiently in the form of a beam is the next step not only toward synthesizing antihydrogen atoms for use in *CPT* symmetry tests [4,5], but also for studying atomic collision dynamics involved in both the formation of antiprotonic atoms and in ionization processes [6,7] and for investigating antiproton-nucleus annihilation in gaseous targets [8]. Since antiproton beams tend to expand along the strongly diverging magnetic field lines at the exit of the solenoid, it is essential to compress the radial size of antiproton clouds in the trap prior to extraction.

Several radial compression techniques are known for a charged particle cloud in an electromagnetic trap. For an ensemble of independent charged particles, a so-called sideband cooling technique can be applied [9–11], which involves irradiating the cloud with a frequency $f_s = f_z + f_m$, f_z being the frequency of the bounce motion along the magnetic field and f_m the magnetron frequency. For non-neutral plasmas, a rotating electric field is applied at a frequency tuned to a plasma mode [12]or a rigid rotation frequency [13]. Furthermore, for pure electron or positron plasmas, a so-called strong drive technique [14–16] has been used. In this case a rotating electric field is applied without tuning to any plasma mode. The above-mentioned techniques have often been effective under a moderately high vacuum, typically 10^{-7}–10^{-6} Pa, at which residual gas atoms still play a role as energy absorbers [17]. Under ultrahigh vacuum (UHV) conditions, electron or positron plasmas can also be cooled via their synchrotron radiation in the strong magnetic field. In the case of antiproton clouds, where UHV conditions are essential to avoid annihilation of the antiprotons, and synchrotron radiation cooling is completely negligible, it has been assumed that use of the strong drive technique is difficult ($p \leq 10^{-10}$ Pa). In this Letter, we present the first experimental demonstration of radial compression of antiproton clouds by a rotating electric field under UHV conditions.

Antiprotons at 5 MeV from the CERN Antiproton Decelerator (AD) were slowed down to 115 keV by a Radio Frequency Quadrupole Decelerator and then were accumulated and cooled in a so-called multiring trap (MRT) [18]. Figure 1 shows a schematic drawing of the experimental setup downstream of the Radio Frequency Quadrupole Decelerator: the MRT housed in a 2.5 T superconducting solenoid, the transport beam line, and a microchannel plate with a delay line anode used as a position sensitive detector (PSD). The MRT consists of 14 ring electrodes, the central five of them being used to form a harmonic potential along the trap axis [15]. One of the ring electrodes was azimuthally segmented into four parts to

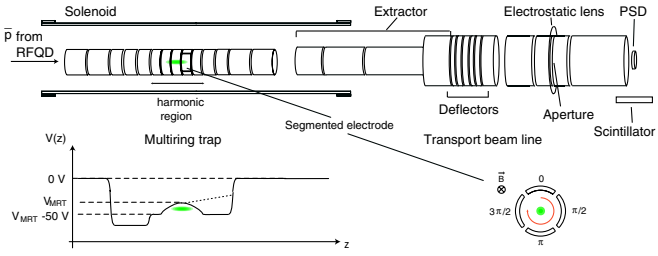

FIG. 1 (color online). A schematic view of the main part of the experimental setup (not to scale) including the multiring trap with a cross section of the segmented electrode (right lower figure) and the transport beam line. Antiprotons ($\bar{p}s$) come from the left side. The left lower figure shows the potential distribution along the axis (z). The dotted line shows the potential distribution during the antiproton extraction. The trap potential depth was 50 V.

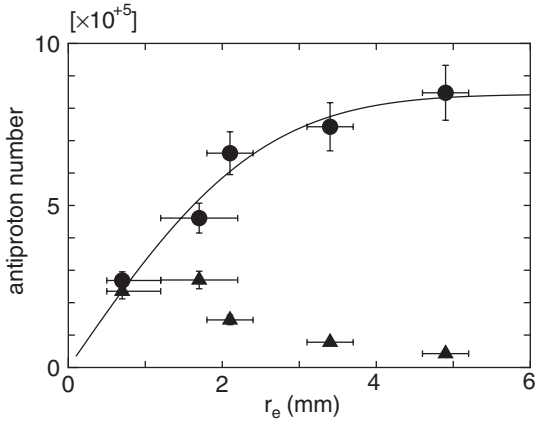

FIG. 2. The number of trapped (solid circles) and transported (solid triangles) antiprotons as a function of the electron plasma radius, r_e. A 2-MHz field was applied with its amplitude $V_r = 1.1$ V, to expand the plasma to a radial size ranging from $r_e \sim 0.8$ to 5 mm. The corresponding volume density of the plasma of 3×10^8 electrons varied from $2.7 \times 10^9/\mathrm{cm}^3$ to $6.5 \times 10^7/\mathrm{cm}^3$, and the length from 62 to 45 mm. The solid line is the best fit to the solid circles, assuming that the radial distribution of the incoming antiproton beam can be expressed by a Gaussian function $\rho(r_{\bar{p}}) = \exp\{-(r_{\bar{p}}/a_{\bar{p}})^2/2\}$, for $a_{\bar{p}} = 1.95$ mm. The uncertainty of antiproton number primarily comes from the fluctuation of the antiproton beam intensity from the AD. The uncertainties of r_e mainly comes from the uncertainty of the plasma oscillation frequencies [3].

which a radio frequency field with phases shifted by $\pi/2$ rad from one segment to another was applied, thereby generating a rotating electric field within the MRT.

Prior to antiproton injection, an electron plasma was prepared in the harmonic region of the MRT. Such an electron plasma is known to have a spheroidal shape with a uniform density and to be controlled with the strong drive technique. The radius and the aspect ratio of the plasma were evaluated nondestructively by measuring eigenmode frequencies of the plasma [3]. The antiprotons were then captured and cooled to sub-eV kinetic energies through interaction with the electron plasma. We measured the number of trapped antiprotons as a function of the radius r_e of the electron plasma [15]. As shown by the solid circles in Fig. 2, the number increased monotonically with r_e and saturated for ≥ 5 mm. Assuming that only the antiprotons overlapping with the electron plasma can be cooled, and that the radial distribution of the incoming antiproton beam can be expressed by a Gaussian function $\rho(r_{\bar{p}}) \propto \exp\{-(r_{\bar{p}}/a_{\bar{p}})^2/2\}$, the experimental result was reproduced satisfactorily with $a_{\bar{p}} = 1.95$ mm, as shown by the solid line in Fig. 2. During the experiments described below, we set $r_e = 3.4$ mm unless otherwise specified. It should be noted that the cooling electrons were kicked out before any further manipulation by opening the MRT for a short time repeatedly [19].

Antiprotons were then extracted and transported to the magnetic-field-free region through x and y deflectors and an electrostatic lens with an aperture of 6 mm in diameter. The lower left part of Fig. 1 shows the potential distribution along the axis. The potential of the MRT V_{MRT} corresponded to the kinetic energy of the extracted antiproton beam. The annihilation position along the beam line was determined by a track detector consisting of two 2-m-long plastic scintillator bars [3] installed parallel to the beam line. The profile of the antiproton beam was monitored by the PSD placed 1.75 m downstream from the center of the MRT. An additional plastic scintillator plate near the PSD identified the antiprotons by detecting passage of annihilation products such as energetic pions.

The triangles in Fig. 2 show the number of extracted antiprotons detected by the PSD as a function of the radius r_e of the preloaded electron plasma. If the radial distribution of the antiproton cloud stays constant during the cooling process, this number should also increase monotonically. In fact, the number decreased for larger electron plasma radius, which showed that the antiproton cloud had expanded radially.

Figures 3(a)–3(d) show the annihilation distribution along the transport beam line. When no rotating field was applied [Fig. 3(a)], most of the antiprotons annihilated around the extractor at the exit of the superconducting solenoid. Figures 3(b)–3(d) correspond to the cases where a rotating electric field with its frequency $f = 247$ kHz was applied for $t_r = 60$, 120, and 200 s, respectively. The annihilation peak around the extractors diminished while the peak around the PSD increased in size as t_r became longer. The corresponding 2D images on the PSD are shown in Figs. 3(e)–3(h). Without the rotating field [case (a)], the image is dim with low intensity and shows a depopulated region (hollow) in its center. This hollow gradually fills up as the field is applied, as in the cases (b), (c), and (d). The antiproton cloud was therefore effectively being compressed by the rotating field. The compressed cloud remained stable in the MRT for at least a few minutes.

Figure 4 shows the measured transport efficiency $\varepsilon_{\mathrm{exp}}$, defined as the ratio of the number of antiprotons detected by the PSD to the number of trapped antiprotons, as a function of t_r. The efficiency $\varepsilon_{\mathrm{exp}}$ monotonically increased from 0.08 for $t_r = 0$ to 0.4–0.45 for $t_r \geq 200$ s. The maximum number of transported antiprotons was about 5×10^5 when 1.1×10^6 antiprotons were captured. Some antiprotons were lost during the compression. The loss rate was twice as large with the rotating field and caused 10% loss of the trapped antiprotons for $t_r = 200$ s.

We performed trajectory simulations to relate the radial distribution of the antiproton cloud in the MRT with the annihilation distribution along the beam line and the image on the PSD. Figures 5(a) and 5(d) show the simulated position distribution of antiproton annihilation and the beam profile at the PSD, respectively, for an antiproton cloud with $a_{\bar{p}} = 3.40$ mm in the MRT. The annihilation

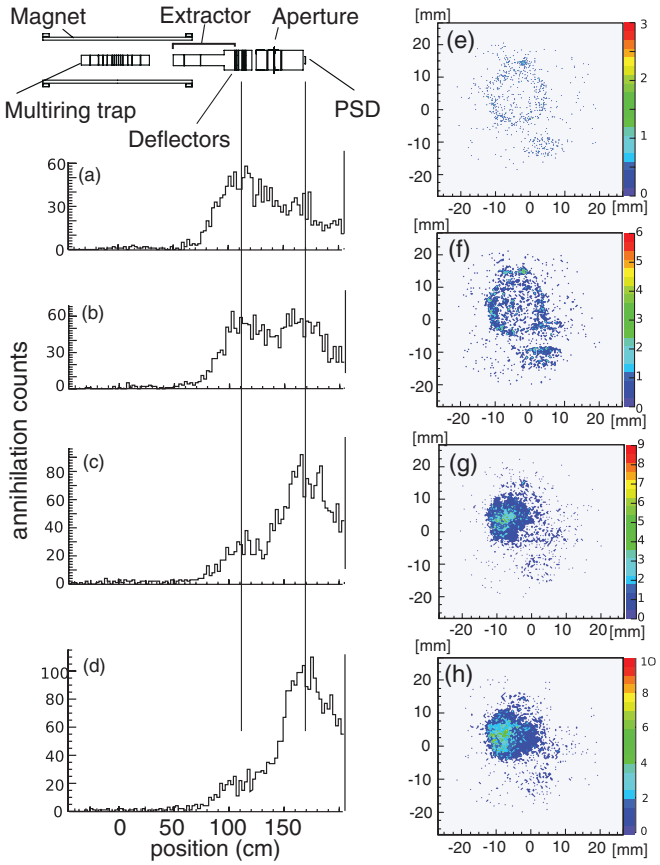

FIG. 3 (color). (a)–(d) The annihilation position of extracted antiprotons along the transport beam line for the rotation time of $t_r = 0$, 60, 120, and 200 s. (e)–(h) The PSD images of extracted antiprotons for $t_r = 0$, 60, 120, and 200 s. The rotation frequency was $f = 247$ kHz with its peak-to-peak amplitude $V_r = 0.56$ V. The electron plasma used had a radius of 3.4 mm and was removed from the MRT before application of the rotating field and the extraction.

distribution in Fig. 3(a) as well as the hollowed distribution of Fig. 3(e) was reproduced reasonably well by the simulation. The calculated efficiency of $\varepsilon_{\mathrm{sim}} = 0.06$ was also consistent with the experimental value of $\varepsilon_{\mathrm{exp}} = 0.08$. This agreement is another indication that the antiproton cloud had expanded to the size of the electron cloud of 3.40 mm from its initial size of $a_{\bar{p}} = 1.95$ mm.

The PSD image in Fig. 3(h) was best reproduced at $a_{\bar{p}} = 0.25$ mm, as shown in Fig. 5(e). On the other hand, the shoulder around the annihilation position of 100 cm in Fig. 3(d) was not seen in Fig. 5(b), and the simulated transport efficiency predicted $\varepsilon_{\mathrm{sim}} \sim 1$, while the experimental value was 0.45 at most. We therefore conclude that the antiproton cloud in the MRT after compression consists of two components. Figures 5(c) and 5(f) show the results of our simulation assuming one component has $a_{\bar{p}} = 0.25$ mm including 45% of antiprotons and $a_{\bar{p}} = 4.0$ mm including 55%, which reproduces the observation in Figs. 3(d) and 3(h), respectively.

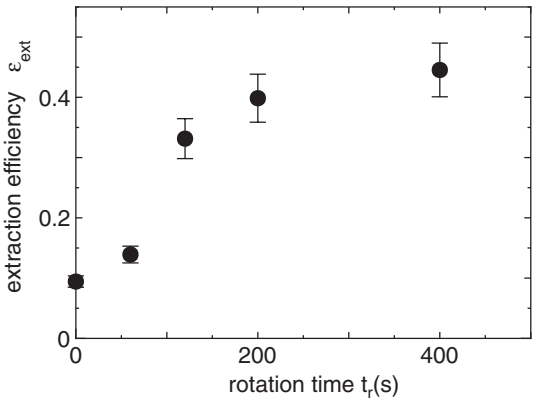

FIG. 4. The transport efficiency $\varepsilon_{\mathrm{exp}}$ of antiprotons as a function of the rotation time t_r for $f = 247$ kHz and $V_r = 0.56$ V. The error bars mainly come from the fluctuation of the antiproton beam intensity from the AD.

Figure 6(a) shows the transport efficiency $\varepsilon_{\mathrm{exp}}$ as a function of the rotation frequency from -250 kHz to 1000 kHz for $t_r = 120$ s and $V_r = 0.56$ V. The negative frequency refers to the counter-rotating field. The transport efficiency appears to be roughly constant at around 0.3 for

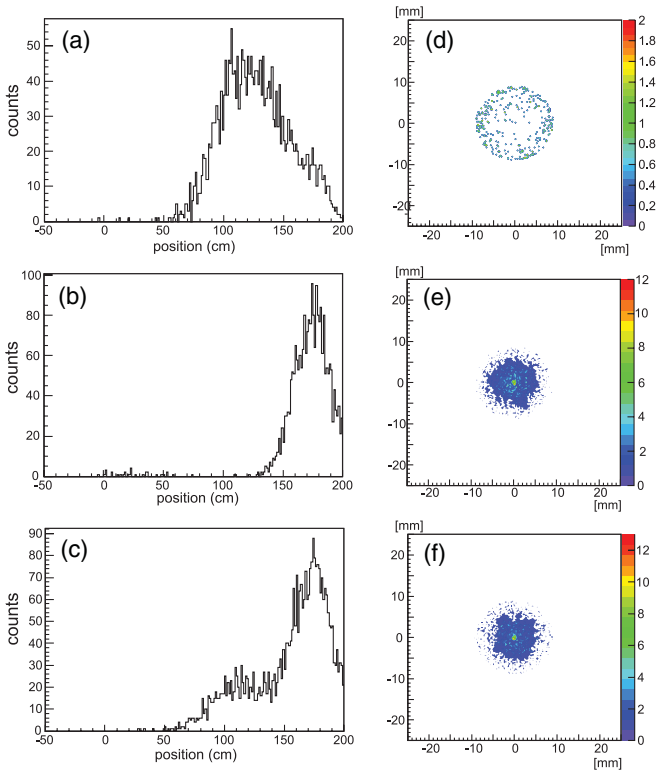

FIG. 5 (color). Simulated antiproton annihilation position distributions along the transport beam line [(a)–(c)] and antiproton beam profiles at the PSD [(d)–(f)]. (a) and (d) $a_{\bar{p}} = 3.4$ mm, (b) and (e) $a_{\bar{p}} = 0.25$ mm, (c) and (f) a superposition of two Gaussian distributions, 45% of $a_{\bar{p}} = 0.25$ mm and 55% of $a_{\bar{p}} = 4.0$ mm.

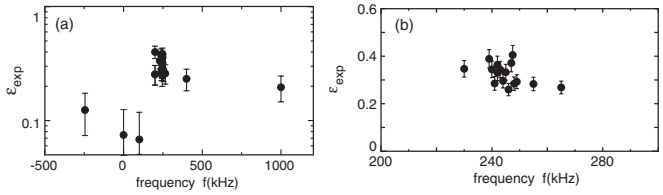

FIG. 6. The transport efficiency ε_{exp} of antiprotons as (a) a function of the rotating field frequency f, and (b) in expansion around $f = 247$ kHz and $t_r = 120$ s. The negative frequency refers to the counter-rotating field. The error bars mainly come from the fluctuation of the antiproton beam intensity from the AD.

$f \geq 200$ kHz. For $f \leq 100$ kHz and lower, the efficiency was approximately the same as it was without rotation. As shown in Fig. 6(b), the frequency dependence was further studied carefully around $f_s = 247.5$ kHz, the sideband frequency for the harmonic potential depth of 50 V. No structure was observed around f_s. A proton cloud of $\sim 1 \times 10^6$ at temperature ~ 5 eV in a vacuum of $\sim 10^{-7}$ Pa [10] was resonantly compressed at the sideband frequency, and thus behaves like an ensemble of independent particles. The amplitude dependence was also studied. This revealed that the transport efficiency was constant for $V_r \geq 50$ mV. These experimental findings indicate that the antiproton compression observed here is phenomenologically similar to the strong drive compression observed for electron plasmas [14–16] rather than the sideband cooling for the proton cloud in higher temperature [10].

The temperature T of the compressed antiproton cloud for $t_r = 200$ s and $V_r = 1.0$ V was evaluated from the number of antiprotons, N, leaking toward the PSD when the potential barrier, ϕ, of the MRT was decreased [20]. Assuming the antiproton cloud is in thermal equilibrium with a Maxwell distribution, the equation $d \log N/d\phi = 1.05e/k_B T$ [20] is satisfied, where k_B is the Boltzmann constant and e is the elementary electric charge. The temperature obtained was $k_B T \lesssim 0.3$ eV—more than 1 order of magnitude lower than the proton cloud discussed in the previous paragraph. The Debye length is around 0.23 mm for the compressed cloud of 5×10^5 antiprotons at 0.3 eV in radius of 0.25 mm, which is compared with 23 mm for the cloud of 1×10^6 protons at 5 eV in radius of 10 mm. This indicates that the antiproton cloud here is more like a plasma than an ensemble of independent particles, which is consistent with the frequency dependence discussed in the previous paragraph.

In summary, we have found an effective compression method for antiprotons trapped in an ultrahigh vacuum of $p \leq 10^{-10}$ Pa. A rotating electric field over a broad frequency range of 200–1000 kHz successfully compressed a half of the antiproton cloud ($5 \times 10^5 \bar{p}$) from 3.4 mm to 0.25 mm in 200 s. Elucidation of the compression mechanism in the UHV condition remains a subject for future studies.

This work was supported by the Grant-in-Aid for Creative Scientific Research (No. 10P0101) of the Japanese Ministry of Education, Culture, Sports, Science and Technology (MonbuKagaku-shō), Special Research Projects for Basic Science of RIKEN, and the Hungarian National Science Foundation (No. OTKA T046095).

[1] G. Gabrielse, Adv. At. Mol. Opt. Phys. **50**, 155 (2005).
[2] M. Charlton *et al.*, Phys. Rep. **241**, 65 (1994).
[3] N. Kuroda *et al.*, Phys. Rev. Lett. **94**, 023401 (2005).
[4] E. Widmann *et al.*, in *The Hydrogen Atom; Precision Physics of Simple Atomic Systems*, edited by S. Kahrhenboim, Lecture Notes in Physics Vol. 570 (Springer Verlag, Heidelberg, 2001), p. 528.
[5] A. Mohri and Y. Yamazaki, Europhys. Lett. **63**, 207 (2003).
[6] Y. Yamazaki, Nucl. Instrum. Methods Phys. Res., Sect. B **154**, 174 (1999).
[7] H. Knudsen and J. Reading, Phys. Rep. **212**, 107 (1992).
[8] E. Lodi Rizzini *et al.*, in *Workshop on Physics with Ultra Slow Antiproton Beams*, edited by Y. Yamazaki and M. Wada, AIP Conf. Proc. Vol. 793 RIKEN (AIP, New York, 2005), p. 183.
[9] L. Brown and G. Gabrielse, Rev. Mod. Phys. **58**, 233 (1986).
[10] H. Higaki *et al.*, Phys. Rev. E **70**, 026501 (2004).
[11] A. Kellerbauer *et al.*, Phys. Rev. A **73**, 062508 (2006).
[12] E. Hollmann, F. Anderegg, and C. Driscoll, Phys. Plasmas **7**, 2776 (2000).
[13] X.-P. Huang *et al.*, Phys. Rev. Lett. **78**, 875 (1997).
[14] J. Danielson and C. Surko, Phys. Rev. Lett. **94**, 035001 (2005).
[15] N. Kuroda *et al.*, in *Workshop on Physics with Ultra Slow Antiproton Beams*, edited by Y. Yamazaki and M. Wada, AIP Conf. Proc. Vol. 793 RIKEN (AIP, New York, 2005).
[16] L. V. Jørgensen *et al.*, Phys. Rev. Lett. **95**, 025002 (2005).
[17] R. Greaves and C. Surko, Phys. Rev. Lett. **85**, 1883 (2000).
[18] A. Mohri *et al.*, Jpn. J. Appl. Phys. **37**, 664 (1998).
[19] Compression together with electrons was tried at rotation frequencies for electron plasma ($f = 2$–3 MHz). This did not work in the amplitude range employed, but further surveys are in progress.
[20] B. Beck, J. Fajans, and J. Malmberg, Phys. Rev. Lett. **68**, 317 (1992).